LETTER

On the positive and negative damping effect of piezoelectric structure using switched-mode bidirectional energy conversion circuit

To cite this article: Bao Zhao *et al* 2023 *Smart Mater. Struct.* **32** 01LT01

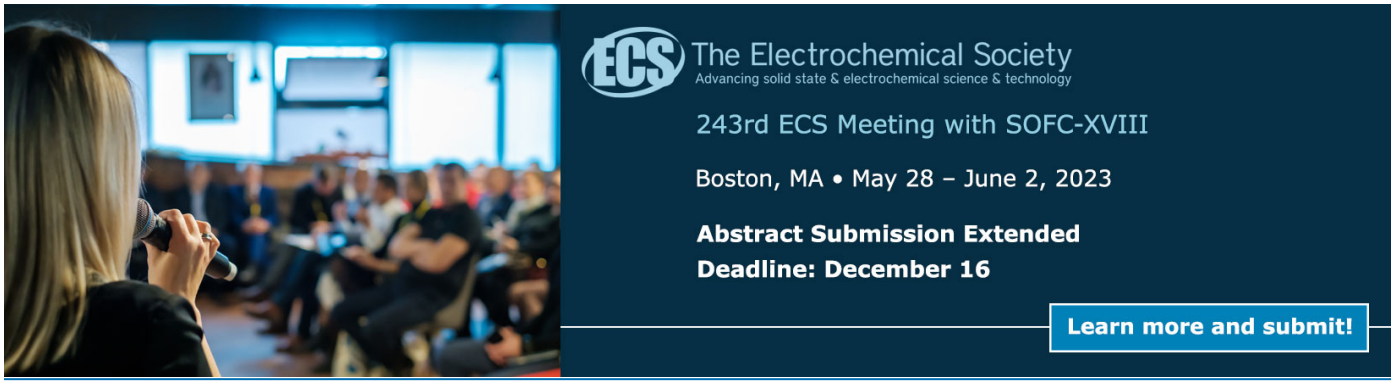

Letters
IOP Publishing
Smart Materials and Structures
Smart Mater. Struct. 32 (2023) 01LT01 (6pp)
https://doi.org/10.1088/1361-665X/aca941

Letter

On the positive and negative damping effect of piezoelectric structure using switched-mode bidirectional energy conversion circuit

Bao Zhao[1], Shiyi Liu[1], Wei-Hsin Liao[2,*] and Junrui Liang[1,3,*]

[1] School of Information Science and Technology, ShanghaiTech University, 393 Middle Huaxia Road, Shanghai 201210, People's Republic of China
[2] Department of Mechanical and Automation Engineering, The Chinese University of Hong Kong, Shatin, Hong Kong, People's Republic of China
[3] Shanghai Engineering Research Center of Energy Efficient and Custom AI IC, Shanghai 201210, People's Republic of China

E-mail: whliao@cuhk.edu.hk and liangjr@shanghaitech.edu.cn

Received 15 August 2022, revised 21 November 2022
Accepted for publication 6 December 2022
Published 14 December 2022

Abstract

The introduction of a switched-mode bidirectional energy conversion circuit (BECC) facilitates the development of piezoelectric devices toward integrated and energy-efficient multi-functional designs. These new designs realize the organic combinations of two or more functions among energy harvesting (EH), vibration excitation (VE), and dynamic sensing. Yet, the structural effect after applying the BECC was not comprehensively investigated and strictly quantified. This letter analyzes the electromechanical joint dynamics of a piezoelectric structure using the BECC, which was developed after the synchronized triple bias-flip (S3BF) technique, under different EH and VE operation modes. It shows that the EH modes electrically induce an extra positive damping effect, while the VE modes induce a negative one. A lumped model and impedance analysis are used to evaluate the electrically induced damping and the energy conversion efficiency by the BECC. The closed-form expression of the vibration displacement under different operation modes is derived. Experiments are carried out under different operation modes and frequencies. The theoretical and experimental results show good agreement. They validate the damping tuning capability of BECC in either positive or negative damping directions. This switched-mode interface circuit offers a promising solution for building an adaptive dynamic control of piezoelectric structures with high energy efficiency.

Keywords: piezoelectric structure, bidirectional energy conversion circuit, dynamic analysis, structural damping

(Some figures may appear in colour only in the online journal)

* Authors to whom any correspondence should be addressed.

1. Introduction

As one of the most extensively utilized electromechanical transducers, piezoelectric transducers can be made into different engineering products, such as sensors, actuators, and small-scale power generators (energy harvesters). Given the conservation of energy, in all piezoelectric designs, the energy is either converted from mechanical to electrical form or in the opposite direction. Power electronics enable more efficient and flexible power conversion in different power levels, from micro-watt to kilo-watt [1]. A trend of deeper fusion between piezoelectric structure and power electronics is observed in recent years [2–4]. More complex switched-mode circuits were designed, enlightening more versatile applications of piezoelectric devices.

The multi-functional concept was observed in some recently proposed designs. Some studies combined either two of the actuation [5, 6], energy harvesting (EH) [4, 7–9], and sensing [10] functions for realizing the compact and integrated piezoelectric solutions, e.g. self-sensing actuation designs [11, 12], optimized actuation by nonlinear circuit design [13], and time-sharing vibration excitation (VE) and EH design [14]. Guyomar *et al* proposed the concept of a self-powered autonomous wireless transmitter/receiver system for the nondestructive evaluation (NDE) purpose [15]. In their design, the EH and VE functions were realized by different circuit modules and separated piezoelectric elements. To integrate different functions in a single circuit, Zhao *et al* proposed the bidirectional energy conversion circuit (BECC), which carries out EH and VE functions in a time-sharing manner [14, 16]. The proposed circuit can be utilized in nonlinear vibration systems to carry out self-powered orbit jumps, with which more energy can be harvested within the frequency hysteresis range [17]. Moreover, Gao *et al* recently proposed the multi-functional piezoelectric circuit [18], which integrates all the dynamic sensing, EH, and VE functions toward more versatile applications. All of the aforementioned multi-functional designs extend the dimensions in engineering design toward self-contained and robust system-level solutions.

The principle of the BECC based on a synchronized triple bias-flip (S3BF) interface circuit [19] was introduced in [14], with a detailed analysis and quantification of the energy conversion process. On the other hand, given that a piezoelectric transducer connects the mechanical and electrical domains, the process of energy conversion is accompanied by the variation of the system's dynamic behavior. The BECC can not only alter the energy flow but also provide a dynamic control to piezoelectric structures. Since switched-mode power electronics are used, this BECC solution is more energy-efficient than the previous op-amp-based designs for resistance or impedance tuning [20, 21].

In this letter, we provide theoretical and experimental studies on the dynamics, specifically, the damping effect, of a piezoelectric structure, when applying the BECC and different operation controls. The dynamics analysis of BECC builds a theoretical foundation for the potential applications in energy-efficient and multi-functional electromechanical systems, e.g. nonlinear energy harvesters [15] and vibration-powered NDE devices [22, 23].

2. Energy flow and damping effect

As shown in figure 1, in any piezoelectric interface circuit, there are three possible energy flows, i.e. the energy flow to the piezoelectric transducer (denoted as ΔE_t in the yellow branch), that to the energy storage device (ΔE_s in green branch), and that dissipated into heat by the parasitic resistance (ΔE_d in orange branch). Given the conservation of energy, for this electromechanically coupled piezoelectric system, we have $\Delta E_t + \Delta E_s + \Delta E_d = 0$. The aforementioned BECC is a special kind of piezoelectric interface circuits, which either converts $-\Delta E_t$ into ΔE_s (EH mode as shown in figure 1(b)) or, the other way around, $-\Delta E_s$ into ΔE_t (VE mode as shown in figure 1(c)). The forward and reverse energy conversions cannot happen simultaneously. They operate in a time-sharing manner. The four operation modes realized by the S3BF-based BECC are briefed in table 1. The EH modes make the piezoelectric voltage v_{p} in phase with the equivalent current i_{eq}, while the VE modes make it out of phase with i_{eq}. The product of v_{p} and i_{eq} is the power extracted from the mechanical structure.

It was well studied that an ideal EH solution introduces a (positive) electrically induced damping effect to the vibrating structure [24–26], which is denoted as D_{e} in figure 2(a). The mechanical lumped model in figure 2(a) is a complementary version of that in [24] after considering the detailed dynamics in practical implementations [27]. Although a general piezoelectric structure might not only behave as a damper under different interfaces and control. This paper focuses on the dynamic effect when connected to the BECC, which specifically produces either a positive (EH mode) or negative (VE mode) damping effect. Therefore, when executing the EH operation with the BECC, the total damping increases beyond its intrinsic mechanical damping D. Moreover, since different EH modes carried out by the BECC have different intensities in energy extraction [14], by running the EH programs, the total damping can be tuned in the positive direction within some extent. As a result, if the base excitation remains the same, the vibration magnitude will be reduced under the EH mode, as illustrated in figure 1(b).

Besides the EH modes, the BECC can also run the VE modes, in which energy is pumped from the storage device to the transducer, i.e. the piezoelectric structure. Such actuation counteracts the intrinsic mechanical damping and enlarges the vibration magnitude under the same base excitation, as illustrated in figure 1(c). In this letter, this counteraction to the intrinsic damping is summarized by a negative damping coefficient, which is still denoted as D_{e} but provided a negative number. In this way, the dynamic effect of the BECC under both the EH and VE modes can be uniformly described.

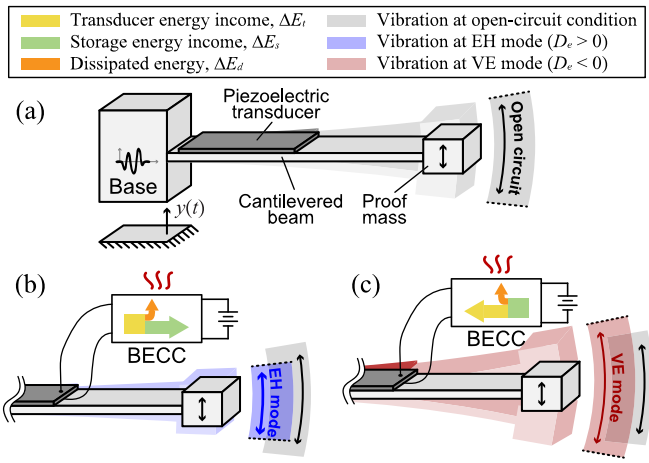

Figure 1. A piezoelectric structure using BECC under: (a) open-circuit condition. (b) EH mode (damping increased), (c) VE mode (damping reduced).

Table 1. BECC operation modes.

Operation mode	Conducting switches for v_p bias-flip actions	
	at i_h falling edge	at i_h rising edge
S1BF-EH	S_1, S_6	S_2, S_3
S3BF-EH	$S_1, S_6 \rightarrow S_2$, $S_6 \rightarrow S_2, S_4$	$S_2, S_3 \rightarrow S_2$, $S_5 \rightarrow S_1, S_5$
S1BF-VE	S_1, S_5	S_2, S_4
S3BF-VE	$S_1, S_5 \rightarrow S_2$, $S_4 \rightarrow S_1, S_5$	$S_2, S_4 \rightarrow S_1$, $S_5 \rightarrow S_2, S_4$

The detailed operation and power evaluation of series-S3BF and its derivative BECC were introduced in [14, 16].

3. Dynamics analysis

The BECC introduces tunable damping to the electromechanically coupled system. The damping contribution can be quantified based on harmonic analysis [28]. In the previous studies of shunt damping or EH, the power conditioning circuit induces positive damping to the system [29], while in some VE studies, the circuit induces a negative equivalent damping to the system [20]. BECC provides an integrated and flexible solution enabling a wide range of damping tunability from positive to negative values. In this section, an equivalent impedance model based on harmonic analysis is derived for a better understanding and evaluation of the dynamic effect of BECC.

The piezoelectric cantilever beam shown in figure 1(a) is excited by a harmonic base acceleration $\ddot{y}(t)$ near its first resonant frequency. The beam dynamics is approximated by an equivalent lumped model, which consists of mass M, damping D, and stiffness K, as illustrated in figure 2(a). The piezoelectric patch and its connected BECC introduce three dynamic components to the system: an open-circuit stiffness K_p, an electrically induced damping D_e, and additional damping D_p equivalently induced by the dielectric dissipation [27]. In practical piezoelectric transducers, usually we have $D_p \gg K_p/\omega$.

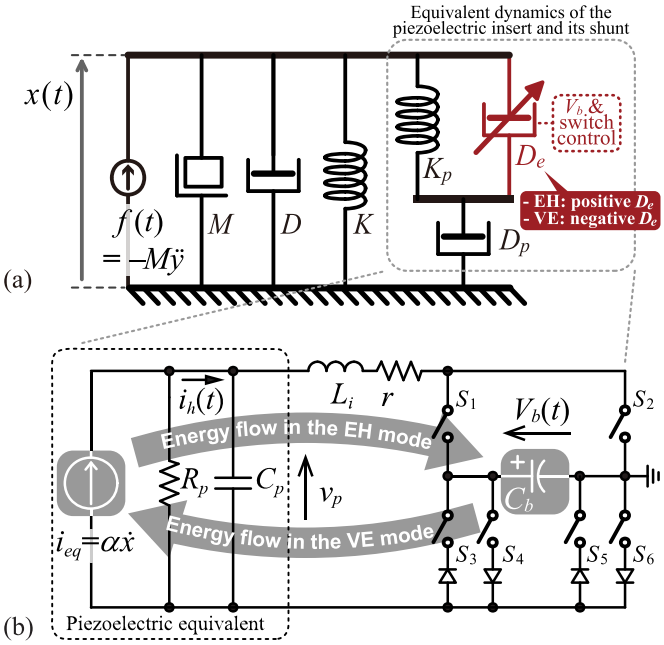

Figure 2. Lumped model of a piezoelectric system. (a) Mechanical schematic; (b) equivalent impedance network of the piezoelectric insert and shunt BECC.

Assuming this much-greater condition holds, the lower end of K_p can be regarded as connecting to the ground in the preliminary analysis. The detailed implementation of BECC is shown in figure 2(b) [14]. It was derived based on the S3BF interface circuit topology [16], which can realize two EH and two VE modes by modifying the switch control logic in every synchronized instant. As shown by the gray arrows in figure 2(b), the circuit transfers energy from the piezoelectric current source i_{eq} to the storage capacitor C_p in the EH mode, and in the opposite direction in the VE mode. The red dashed frame in figure 2(a) indicates that the value of D_e is related to the bias voltage V_b and switch control.

The BECC dynamics can be studied based on the equivalent circuit shown in figure 2(b). Given that i_h the current flowing through the C_p and BECC combination is a harmonic function

$$i_h(t) = I_h \sin(\omega t), \tag{1}$$

where I_h is the current magnitude; ω is the vibration frequency. No matter under any EH or VE mode, the voltage across the piezoelectric element can be formulated with a piecewise equation as follows

$$v_p(t) = \begin{cases} V_{oc}[1-\cos(\omega t)] - V_M(V_b,\gamma), & 0 \leqslant \omega t < \pi; \\ V_M(V_b,\gamma) - V_{oc}[1+\cos(\omega t)], & \pi \leqslant \omega t < 2\pi, \end{cases} \tag{2}$$

where $V_{oc} = I_h/(\omega C_p)$ is the open circuit voltage magnitude, V_M is the final voltage after the Mth bias-flip actions in each current zero-crossing instant from positive to negative i_h [14].

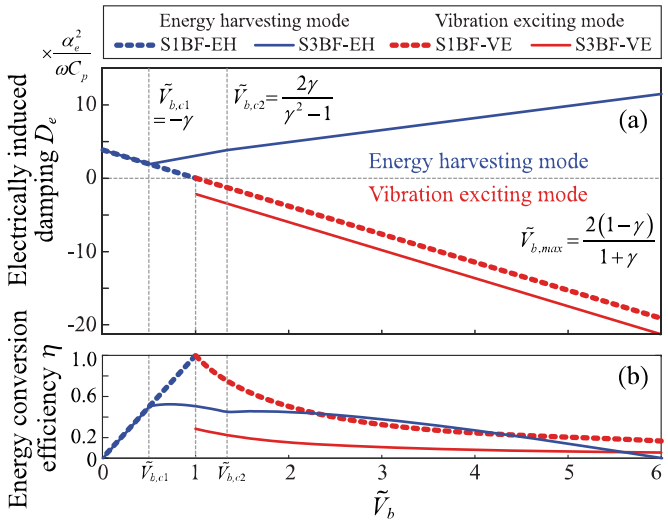

Figure 3. (a) Electrically induced damping effect and (b) energy conversion efficiency under different non-dimensionalized bias voltage $\tilde{V}_\mathrm{b}$ (flipping factor $\gamma=-0.5$).

It can be expressed as a function of the bias voltage V_b and flipping factor γ according to different operation modes [14].

By studying the magnitude and phase relation between the fundamental harmonic of v_p and i_h [27], we can formulate the equivalent impedance of the clamped capacitor C_p and BECC combination in the frequency domain as follows

$$Z_e(j\omega)=\frac{V_{p,f}(j\omega)}{I_h(j\omega)}=\frac{1}{\omega C_\mathrm{p}}\left[\frac{4}{\pi}\left(1-\tilde{V}_M\right)-j\right], \tag{3}$$

where $I_h(j\omega)$ and $V_{p,f}(j\omega)$ are the frequency-domain expressions of i_h and that of the fundamental harmonic of v_p, respectively; $\tilde{V}_M=V_M/V_\mathrm{oc}$ is a non-dimensional V_M. The imaginary part of Z_e is a constant number. By taking the electromechanical analogy, it corresponds to an electrically induced stiffness in the mechanical domain, i.e.

$$K_\mathrm{p}=\alpha^2/C_\mathrm{p}=-\alpha^2\omega\,\mathrm{Im}[Z_\mathrm{e}], \tag{4}$$

where α is the force-voltage coupling factor, which describes the coupling intensity of the piezoelectric structure. On the other hand, R_e the real part of Z_e is a tunable resistive component related to $\tilde{V}_\mathrm{b}=V_\mathrm{b}/V_\mathrm{oc}$ through $\tilde{V}_M$. The flipping factor γ is fixed after circuit manufacturing. In the mechanical domain, it corresponds to an electrically induced damping

$$D_\mathrm{e}=\alpha^2R_\mathrm{e}=\alpha^2\,\mathrm{Re}[Z_\mathrm{e}]. \tag{5}$$

Figure 3(a) shows the picture of D_e as a function of $\tilde{V}_\mathrm{b}$ under different BECC operation modes. In the EH modes (blue curves), D_e is positive. S3BF-EH makes larger D_e compared with S1BF-EH. Therefore, the EH capability of S3BF-EH is stronger. In the VE modes, D_e is negative. Therefore, the total damping is reduced by adding D_e to the mechanical damping D. Compared with S1BF-VE, S3BF-VE mode can further reduce the electrically induced damping under the same $\tilde{V}_\mathrm{b}$. This implies that S3BF-VE has a stronger excitation capability compared with S1BF-VE.

Damping reduces the vibration magnitude by removing energy from the electromechanical system. The energy extracted from the piezoelectric transducer, i.e. negative transducer energy income, in one vibration period $T=2\pi/\omega$ can be formulated as follows

$$-\Delta E_t=\int_T v_p(t)\,i_h(t)\,\mathrm{d}t=\frac{\pi I_h^2R_\mathrm{e}}{\omega}. \tag{6}$$

The detailed expressions of other energy flows ΔE_s and ΔE_d in different operation modes of BECC are documented in [14]. The energy conversion efficiency under either EH or VE mode are defined as follows, respectively,

$$\eta_\mathrm{EH}=\frac{\Delta E_s}{-\Delta E_t},\quad \eta_\mathrm{VE}=\frac{\Delta E_t}{-\Delta E_s}. \tag{7}$$

Given ideal lossless switches and diodes in the switched-mode circuit, figure 3(b) shows the energy conversion efficiencies under different operation modes. For all the cases, maximum conversion efficiency attains around $\tilde{V}_\mathrm{b}=1$. When V_b decreases or increases beyond V_oc, the conversion efficiency decreases due to the quadratic increase of the (electrically) dissipated energy ΔE_d. We must note that the larger conversion efficiency neither implies stronger EH or vibration-exciting abilities, nor better performance, but only a more efficient use of the energy. A larger adjustable span of positive or negative damping, as illustrated by the vertical axis in figure 3(a) is the emphasis of this paper. A higher energy conversion efficiency is not the prior design objective at this stage. Figure 3(b) only gives an idea about the cost-effectiveness of energy usage in this damping tuning solution. In general, within either the EH or VE modes, the triple bias-flip versions, i.e. S3BF-EH or S3BF-VE, produce larger (positive or negative) damping magnitude; yet, they are implemented at lower energy conversion efficiencies, compared with their single bias-flip counterparts, i.e. S1BF-EH or S1BF-VE, respectively. The reason is that, in the bias-flip-based interface circuits, more bias-flip actions lead to more energy dissipation, which lowers the conversion efficiency. However, the net harvested energy in the EH modes or the injected mechanical energy in the VE modes can still increase due to the larger amount of energy extracted from the transducer or from the storage, respectively. The effectively transformed energy (ΔE_s in EH modes or ΔE_t in VE modes) induces the ultimate positive or negative electrically induced damping effect on the electromechanical system.

After the analyses of the electrically induced damping effect and the energy conversion efficiency of BECC, we can further investigate its damping tuning capability in a whole dynamic system. According to the lumped dynamic model shown in figure 2(a), and given the $D_\mathrm{p}\gg K_\mathrm{p}/\omega$ assumption, the governing equation of this system can be written as follows

$$M\ddot{x}(t)+(D+D_\mathrm{e})\dot{x}(t)+(K+K_\mathrm{p})x(t)=-M\ddot{y}(t). \tag{8}$$

D_e is the only tunable equivalent component in operation. Given the harmonic base excitation $y(t)=Y\sin(\omega t)$, where Y is the amplitude. The phase of $y(t)$ has nothing to do with that

in (1) and (2). The harmonic relation in (1) and (2) is only used to derive (3). Solving (8) yields the displacement under steady-state base excitation

$$x(t) = \lambda \frac{M\omega^2 Y}{K} \sin(\omega t - \varphi), \tag{9}$$

where

$$\lambda = \left\{ \left(1 + \mu - \tilde{\omega}^2\right)^2 + \left[2(1+\eta)\zeta\tilde{\omega}\right]^2 \right\}^{-1/2} \tag{10}$$

is the displacement amplification factor, while

$$\varphi = \tan^{-1}\left[\frac{2(1+\eta)\zeta\tilde{\omega}}{1+\mu-\tilde{\omega}^2}\right] \tag{11}$$

is the phase of the forced vibration. In (10) and (11), $\tilde{\omega} = \omega/\omega_n$ is the normalized frequency, where $\omega_n = \sqrt{K/M}$ is the natural frequency. $\eta = \zeta_e/\zeta = D_e/D$ denotes the ratio between electrically induced damping and mechanical damping. $\zeta = D/(2M\omega_n)$ and $\zeta_e = D_e/(2M\omega_n)$ are their corresponding damping ratios. $\mu = K_p/K$ represents the ratio between electrically induced stiffness and mechanical stiffness. Therefore, under the same base excitation, (10) infers that larger electrically induced damping D_e leads to smaller displacement amplitude factor λ.

The analysis mentioned above was based on the $D_p \gg K_p/\omega$ assumption. Equations (8)–(11) give an intuitive understanding about the effect of different induced D_e. In a more accurate power evaluation, we have to turn to the improved model, which considers the effect of finite R_p [27]. The amendment can be done by replacing the K_p and D_e terms in (8) with the following two terms

$$K_p' = -\alpha^2\omega \,\mathrm{Im}\left[\frac{Z_e R_p}{Z_e + R_p}\right], \quad D_e' = \alpha^2 \mathrm{Re}\left[\frac{Z_e R_p}{Z_e + R_p}\right], \tag{12}$$

respectively. A more accurate solution of displacement $x(t)$ is obtained numerically. The frequency responses of the piezoelectric cantilever under different operation modes, which are obtained theoretically with the improved model, are subjected to the experimental validation in section 4.

4. Experiment

Experiments are carried out for validating the dynamics analysis. Figure 4 shows the experimental setup. The piezoelectric cantilever is excited by a vibration exciter (APS420, SPEKTRA GmbH) near the beam's first-mode natural frequency ω_n. Its output electrodes are connected to a BECC interface circuit. A laser vibrometer (OFV-552/5000, Polytec GmbH) is used to measure the relative velocity and displacement between the tip and vibrating base. Since the relative velocity $\dot{x}$ is proportional to the equivalent current i_{eq}, which is very close to i_h under a small dielectric dissipation condition, the velocity signal is also used for synchronizing the bias-flip actions. This is carried out by a micro-controller (MSP430G2553, Texas Instrument Ltd) and some MOSFET switches. Table 2 lists the

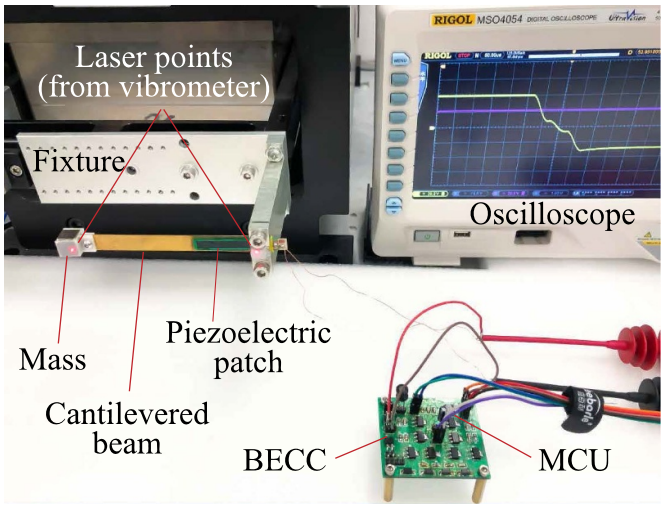

Figure 4. Experimental setup.

Table 2. Parameters of a linear piezoelectric system.

Parameter	Value	Parameter	Value
M	0.009 kg	k_e^2	0.007
D	0.007 Ns m^{-1}	C_b	47 μF
K	52 N m^{-1}	ω_n	$2\pi \times 12.22$ Hz
L_i	10 mH	α	1.13×10^{-4} N V^{-1}
C_p	35.75 nF	Acceleration $\ddot{Y}$	0.5 m s^{-2}
R_p	1.9 MΩ	Diode	SS16
γ	-0.404	MOSFET	ZVP/ZVN4424

parameters of the experimental setup and components used in the experiment.

The displacement amplitudes under different frequencies ($0.9 < \tilde{\omega} < 1.1$) and operation modes in the experiment are recorded after steady state to evaluate the damping tuning ability and validate the theoretical analysis. The load conditions used in experiments are short-circuit for S1BF-EH and open-circuit for S3BF-EH, respectively, to achieve maximum positive electrically induced damping D_e in figure 3(a). An external voltage source is used to provide a constant V_b for the VE modes to produce the corresponding negative electrically induced damping D_e. All results are shown in figure 5. The electrical-to-mechanical damping ratio η varies from positive (in EH modes) to negative (in VE modes). The black curve represents the open-circuit condition, i.e. $\eta = 0$ case. The blue curves show the cases in EH modes, where $\eta > 0$. Compared with the open-circuit condition, the displacement amplitudes are suppressed when the EH modes are activated. The vibration magnitude under S3BF-EH is lower than that under S1BF-EH due to the stronger damping effect by a more intensive EH function. On the contrary, as indicated by the red curves in figure 5, in the VE modes, where $\eta < 0$, the vibration expands. In these cases, the total damping effect is reduced by introducing a negative D_e. Since S3BF-VE can realize a larger VE function than S1BF-VE, its damping reduction capability is more significant. From figure 5, the theoretical results match the experimental data very well. The damping tuning ability

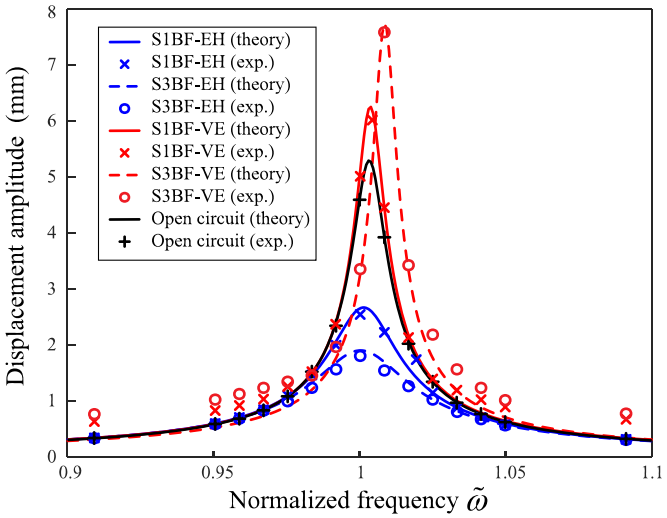

Figure 5. Displacement amplitude under different normalized frequency $\tilde{\omega}$.

of BECC under different operation modes is validated. The maximum displacement amplitudes in S3BF-EH, S1BF-EH, S1BF-VE, and S3BF-VE are 35.9%, 50.4%, 117.9%, and 146.3% to that in open-circuit condition, in which only the inherent mechanical damping is included, respectively. It is worth noting that the total damping decreases from the EH modes to the open-circuit mode and then to the VE modes. The peak of the frequency response function, i.e. the resonant frequency location, shifts along the higher-frequency direction.

5. Conclusion

This letter has provided a timely analysis of the electromechanical joint dynamics of a piezoelectric structure when using the synchronized triple bias-flip (S3BF) based switched-mode BECC. The electrically induced damping effects produced by the BECC under different operation modes, i.e. S1BF-EH, S3BF-EH, S1BF-VE, and S3BF-VE modes, were derived and quantified based on equivalent impedance analysis. With the tunable damping effect, the vibration of a piezoelectric vibrator can be reduced by running the EH modes or magnified by running the VE modes. The experimental results have validated the influence of BECC as theoretical analysis predicted. The dynamics tuning ability of BECC indicates a potential direction toward energy-efficient and multi-functional piezoelectric devices and integrated engineering designs.

Data availability statement

No new data were created or analysed in this study.

Acknowledgment

This work was supported in part by the Natural Science Foundation of Shanghai under Grant 21ZR1442300; in part by the National Natural Science Foundation of China under Grants 62271319 and U21B2002.

ORCID iDs

Wei-Hsin Liao https://orcid.org/0000-0001-7221-5906
Junrui Liang https://orcid.org/0000-0003-2685-5587

References

[1] Erickson R W and Maksimovic D 2007 *Fundamentals of Power Electronics* (New York: Springer)
[2] Brenes A, Morel A, Juillard J, Lefeuvre E and Badel A 2020 *Smart Mater. Struct.* **29** 033001
[3] Zhang B, Liu H, Hu B and Zhou S 2022 *Smart Mater. Struct.* **31** 095040
[4] Morel A, Brenes A, Gibus D, Lefeuvre E, Gasnier P, Pillonnet G and Badel A 2022 *Smart Mater. Struct.* **31** 045016
[5] Deng J, Liu Y, Zhang S and Li J 2021 *IEEE/ASME Trans. Mechatronics* **26** 2059–70
[6] Liu L, Yun H, Li Q, Ma X, Chen S L and Shen J 2020 *IEEE/ASME Trans. Mechatronics* **25** 1036–44
[7] Jung H J, Eshghi A T and Lee S 2021 *IEEE/ASME Trans. Mechatronics* **26** 1708–18
[8] Wang J, Zhao B, Liao W H and Liang J 2020 *Smart Mater. Struct.* **29** 04LT01
[9] Gao Y, Hu G, Zhao B, Lv K and Liang J 2021 *Smart Mater. Struct.* **30** 105023
[10] Kim H, Lee K, Jo G, Kim J S, Lim M T and Cha Y 2021 *IEEE/ASME Trans. Mechatronics* **26** 2538–47
[11] Hu B, Pang C K, Wan J, Cao S, Tan J K, Li H, Wang J and Guo G 2021 *Trans. Inst. Meas. Control* **43** 802–11
[12] Jayaram K, Jafferis N T, Doshi N, Goldberg B and Wood R J 2018 *Smart Mater. Struct.* **27** 065028
[13] Ducharne B, Garbuio L, Lallart M, Guyomar D, Sebald G and Gauthier J Y 2012 *IEEE Trans. Power Electron.* **28** 3941–8
[14] Zhao B, Wang J, Liao W H and Liang J 2021 *IEEE Trans. Power Electron.* **36** 12889–97
[15] Guyomar D, Jayet Y, Petit L, Lefeuvre E, Monnier T, Richard C and Lallart M 2007 *Sens. Actuators* A **138** 151–60
[16] Zhao B, Zhao K, Wang X, Liang J and Chen Z 2020 *IEEE Trans. Power Electron.* **36** 6787–96
[17] Wang J, Zhao B, Liang J and Liao W H 2019 Orbit jumps of monostable energy harvesters by a bidirectional energy conversion circuit *ASME IDETC-CIEC Conf.* vol 59285 p V008T10A016
[18] Gao L, Teng L and Liang J 2021 A switched-mode piezoelectric interface circuit for dynamics sensing, energy harvesting and vibration excitation multi-functional purpose *Proc. SPIE* **11588** 115880W
[19] Zhao B, Zhao K, Wang X, Liang J and Chen Z 2021 *IEEE Trans. Power Electron.* **36** 6787–96
[20] Lan C, Tang L and Qin W 2017 *Eur. Phys. J. Appl. Phys.* **79** 20902
[21] Callanan J, Willey C L, Chen V W, Liu J, Nouh M and Juhl A T 2021 *Smart Mater. Struct.* **31** 015002
[22] Anton S R and Sodano H A 2007 *Smart Mater. Struct.* **16** R1
[23] Safaei M, Sodano H A and Anton S R 2019 *Smart Mater. Struct.* **28** 113001
[24] Williams C B and Yates R B 1996 *Sens. Actuators* A **52** 8–11
[25] Lesieutre G A, Ottman G K and Hofmann H F 2004 *J. Sound Vib.* **269** 991–1001
[26] Shen H, Qiu J and Balsi M 2011 *Sens. Actuators* A **169** 178–86
[27] Liang J, Chung H S H and Liao W H 2014 *Smart Mater. Struct.* **23** 092001
[28] Liang J and Liao W H 2012 *IEEE/ASME Trans. Mechatronics* **17** 1145–57
[29] Kong N, Ha D S, Erturk A and Inman D J 2010 *J. Intell. Mater. Syst. Struct.* **21** 1293–302